CORA Cork Open Research Archive
Cartlann Taighde Oscailte Chorcaí

Title	Nanoscale measurements of phosphorous-induced lattice expansion in nanosecond laser annealed germanium
Authors	Boninelli, Simona;Milazzo, R;Carles, Robert;Houdellier, Florent;Duffy, Ray;Huet, Karim;La Magna, Antonio;Napolitani, E;Cristiano, Fuccio
Publication date	2018
Original Citation	Boninelli, S., Milazzo, R., Carles, R., Houdellier, F., Duffy, R., Huet, K., La Magna, A., Napolitani, E. and Cristiano, F. (2018) 'Nanoscale measurements of phosphorous-induced lattice expansion in nanosecond laser annealed germanium', APL Materials, 6(5), 058504 (7pp). doi: 10.1063/1.5022876
Type of publication	Article (peer-reviewed)
Link to publisher's version	https://aip.scitation.org/doi/10.1063/1.5022876 - 10.1063/1.5022876
Rights	© 2018, the Author(s). All article content, except where otherwise noted, is licensed under a Creative Commons Attribution (CC BY) license (http://creativecommons.org/licenses/by/4.0/). - http://creativecommons.org/licenses/by/4.0/
Download date	2026-11-08 01:10:01
Item downloaded from	https://hdl.handle.net/10468/6846

UCC
University College Cork, Ireland
Coláiste na hOllscoile Corcaigh

Nanoscale measurements of phosphorous-induced lattice expansion in nanosecond laser annealed germanium

S. Boninelli, R. Milazzo, R. Carles, F. Houdellier, R. Duffy, K. Huet, A. La Magna, E. Napolitani, and F. Cristiano

Citation: APL Materials **6**, 058504 (2018); doi: 10.1063/1.5022876
View online: https://doi.org/10.1063/1.5022876
View Table of Contents: http://aip.scitation.org/toc/apm/6/5
Published by the American Institute of Physics

Articles you may be interested in

Perspective: 2D for beyond CMOS
APL Materials **6**, 058202 (2018); 10.1063/1.5022769

Perspective: New process technologies required for future devices and scaling
APL Materials **6**, 058203 (2018); 10.1063/1.5026805

Anisotropic stress in narrow sGe fin field-effect transistor channels measured using nano-focused Raman spectroscopy
APL Materials **6**, 058501 (2018); 10.1063/1.4999277

Preface: Materials, metrology, and modeling for a future beyond CMOS technology
APL Materials **6**, 058001 (2018); 10.1063/1.5037331

Relation between film thickness and surface doping of MoS_2 based field effect transistors
APL Materials **6**, 058301 (2018); 10.1063/1.4996425

In-line metrology for roll-to-roll UV assisted nanoimprint lithography using diffractometry
APL Materials **6**, 058502 (2018); 10.1063/1.5011740

AIP | Conference Proceedings
Get 30% off all print proceedings!
Enter Promotion Code PDF30 at checkout



Nanoscale measurements of phosphorous-induced lattice expansion in nanosecond laser annealed germanium

S. Boninelli,[1] R. Milazzo,[2] R. Carles,[3] F. Houdellier,[3] R. Duffy,[4] K. Huet,[5] A. La Magna,[6] E. Napolitani,[2] and F. Cristiano[7]
[1]*IMM CNR, Dipartimento di Fisica ed Astronomia, Università di Catania, Via S. Sofia 64, 95123 Catania, Italy*
[2]*Dipartimento Fisica, Università di Padova, Via F. Marzolo 8, 35131 Padova, Italy*
[3]*CEMES-CNRS, 29 Rue Jeanne Marvig, 31055 Toulouse, France*
[4]*Tyndall National Institute, University College Cork, Lee Maltings, Cork, Ireland*
[5]*Laser Systems and Solutions of Europe (LASSE), SCREEN Semiconductor Solutions, Co., Ltd., 14-38 Rue Alexandre, 92230 Gennevilliers, France*
[6]*IMM CNR, Zona Industriale, Strada VIII 5, 95100 Catania, Italy*
[7]*LAAS-CNRS, 7 Ave. du Colroy la Roche, F-31400 Toulouse, France*

(Received 19 January 2018; accepted 29 March 2018; published online 17 May 2018)

Laser Thermal Annealing (LTA) at various energy densities was used to recrystallize and activate amorphized germanium doped with phosphorous by ion implantation. The structural modifications induced during the recrystallization and the related dopant diffusion were first investigated. After LTA at low energy densities, the P electrical activation was poor while the dopant distribution was mainly localized in the polycrystalline Ge resulting from the anneal. Conversely, full dopant activation (up to 1×10^{20} cm^{-3}) in a perfectly recrystallized material was observed after annealing at higher energy densities. Measurements of lattice parameters performed on the fully activated structures show that P doping results in a lattice expansion, with a perpendicular lattice strain per atom $\beta_{Ps} = +0.7 \pm 0.1$ Å^3. This clearly indicates that, despite the small atomic radius of P compared to Ge, the "electronic contribution" to the lattice parameter modification (due to the increased hydrostatic deformation potential in the conduction band of P doped Ge) is larger than the "size mismatch contribution" associated with the atomic radii. Such behavior, predicted by theory, is observed experimentally for the first time, thanks to the high sensitivity of the measurement techniques used in this work. © *2018 Author(s). All article content, except where otherwise noted, is licensed under a Creative Commons Attribution (CC BY) license (http://creativecommons.org/licenses/by/4.0/).* https://doi.org/10.1063/1.5022876

Since the early 2000s, there is a renewed interest in the use of germanium in the microelectronics industry, not only as a possible high-mobility replacement for silicon in the CMOS technology[1,2] but also as an interesting candidate for the fabrication of active photonic devices for photon detection, modulation, and generation.[3,4] In most cases, highly doped regions must be combined with tensile strain either to reduce the access resistance or to induce the formation of a direct bandgap in photonic devices.[5,6] However, the introduction of dopant atoms in crystalline materials often results in the generation of stress (and related strain) which depends on the peculiar configuration within the matrix lattice (substitutional or interstitial).[7,8] For this reason, there is a leading technological interest for quantifying the contribution of dopants to the strain. While strain engineering is of interest in many domains such as opto-electronics, photonics, and sensors,[9–11] stresses and strains can have a direct impact on several doping-related phenomena, including the formation of point- and extended defects, dopant solubility and diffusion, and the recrystallization of amorphous layers [Ref. 12 and the references therein]. The nanoscale measurement of crystal strain fields is therefore of high technological and fundamental interest for the understanding of mechanical and optical properties of innovative devices.

In the case of substitutional doping, the formulation of predictive models of doping-induced strain is a complex matter because the theory should compute the dependence of the lattice parameter

 © Author(s) 2018

on two distinct contributions: (i) the well-known "size contribution," governed by the Vegard's law and associated with the covalent radii mismatch between the host matrix and the dopant[13] and (ii) the "electronic contribution," which is associated with the hydrostatic deformation potential induced by the increased carrier population in the conduction band.[14] Although the evidence of this double contribution has been demonstrated for dopants in Si since several decades,[15,16] only recently a strong experimental proof for the Ge case has been provided by Xu *et al.*[8] The experimental approach used by these authors was able to fully confirm the validity of the "double contribution" theory in the case of Sb and As in Ge, while in the case of phosphorus the experimental results were in contradiction with the theoretical predictions. Indeed, despite phosphorus exhibiting a significantly smaller atomic radius compared to Ge, the "double contribution" theory predicts that its inclusion in Ge should generate an expansion of the lattice. Instead, a slightly negative (tensile) deformation was measured in Ref. 8. This was explained by the authors by considering that in the doping interval investigated in that work ($4–7 \times 10^{19}$ cm^{-3}) the magnitude of the expected lattice deformation was too close to the fluctuations of the measured lattice parameter in the reference (i.e., undoped) Ge samples.

In this work, we therefore propose to improve the experimental setup for the investigation of the strain induced by the P doping of germanium in order to demonstrate the validity of the "double contribution" theory also in this case. To this purpose, on the one hand, we increased the expected strain level to be measured by increasing the active dopant concentration up to 1×10^{20} cm^{-3}. This was achieved by combining ion implantation and nanosecond Laser Thermal Annealing (LTA) in the *melt* configuration.[17] Indeed, the ultra-fast solidification of the implanted material from the liquid phase is known to provide a perfect recrystallisation[7] together with dopant activation levels well above the equilibrium limit.[18] On the other hand, two different techniques were used to measure the dopant-induced strain. In addition to High Resolution X-Ray Diffraction (HRXRD), which has proved to be a powerful tool to measure the strain induced by dopants within a crystalline matrix,[19] Convergent Beam Electron Diffraction (CBED) measurements were conducted in the STEM (Scanning Transmission Electron Microscopy) mode so that localized strain measurements could be achieved with nanometer spatial resolution.[20]

In the following, we will first present a detailed structural investigation of the ion implanted and LTA annealed samples, showing how the damage recovery occurs as a function of the LTA conditions. Strain investigations will then be performed in the best samples, both in terms of crystalline quality and dopant activation, and presented in the second part of the paper.

A Ge Czochralski wafer, (100)-oriented, (p-type 0.059–0.088 Ω cm) was implanted with 2×10^{15} P/cm^2 at 15 keV, resulting in the amorphisation of the wafer surface down to about 35 nm. Several 1×1 cm^2 areas of the implanted wafer were subjected to a single pulse LTA treatment at various energy densities, i.e., 0.55, 0.80, 1.05, and 1.20 J/cm^2 (λ = 308 nm, ~106 ns of exposure time), to recrystallize the amorphous layer and electrically activate the dopant. The chemical P profiles were measured by Secondary Ion Mass Spectrometry (SIMS) using a CAMECA IMS-4f instrument with a 5.5 keV Cs^+ beam, analyzing $^{133}Cs^{31}P^+$ secondary ions, and a 7.25 keV Cs^+ beam analyzing O^- secondary ions. The concentration of all species was calibrated by using commercial certified standards with an overall accuracy of 10%, and the depth scale was calibrated by measuring the crater depths with a profilometer and assuming constant sputtering rates, with an overall accuracy of 2%. The structural transformations induced by the LTA were investigated by Transmission Electron Microscopy (TEM) and Raman spectroscopy. Conventional TEM analyses were performed on cross section (CS) samples using a 200 keV 2010F JEOL instrument. CS samples were prepared by means of standard preparation with mechanical grinding and ion milling performed in a GATAN-PIPS apparatus at a low energy (3 keV Ar^+) and low incidence angle (7°) to minimize the irradiation damage. Micro-Raman Stokes spectra were recorded in backscattering geometry with an XploRA Horiba Jobib-Yvon spectrometer. Measurements were performed at low power intensity and by scanning the sample in order to avoid any heating effect. Different exciting laser wavelengths (431, 532, 638, and 785 nm) were used to explore the samples with different light penetration depths. Only the spectra recorded with the 532 nm line are presented in the supplementary material as they ensure the best intensity signal essentially originating (~98%) from the implanted region.

High resolution X-ray diffraction measurements were done using a Philips MRD X-Pert PRO™ system, equipped with a parabolic mirror and a Bartels Ge (220) four-crystal monochromator. In particular, the Cu $K\alpha_1$ radiation (~8 keV) was selected as the probe. The angular acceptance was reduced down to 12 arc sec by a channel-cut (220) analyzer equipped detector. In order to check the strain status, we recorded symmetrical (004) and also asymmetrical (444) reciprocal lattice points. Since no parallel mismatch or tilt with the substrate was observed, we concluded that the doped layer is pseudomorphic in all the samples, i.e., it induces only tetragonal distortion on the Ge host lattice along the direction perpendicular to the regrowth plane. As a result, we focused only on the perpendicular strain $\varepsilon_\perp$ as defined by the formula,

$$\varepsilon_\perp = \frac{a_\perp - a_{rel}}{a_{rel}}, \tag{1}$$

where $a_\perp$ and a_{rel} are the perpendicular and relaxed lattice parameters, respectively. Given the above-mentioned pseudomorphicity, only symmetrical (004) measurements are sufficient to determine $\varepsilon_\perp$ in every sample by making use of elasticity theory,[21]

$$\varepsilon_\perp = -2\frac{C_{12}}{C_{11}}\frac{a_{Ge} - a_{rel}}{a_{rel}}, \tag{2}$$

where a_{Ge} is the Ge lattice constant and C_{11}/C_{12} are its elastic constants.[22] In order to extract $\varepsilon_\perp$ depth profiles, ω-2θ scans (rocking curves, RCs) were measured and then simulated by using the RADS code,[23] which takes into account the XRD dynamical theory. Strain depth profiles with a depth resolution of 10-20 nm and a sensitivity of $\sim 0.2 \times 10^{-5}$ are obtained using this fitting procedure. Finally, CBED was performed in the STEM mode with a sub-nanometer probe using the I2TEM-Toulouse Hitachi cold Field Emission Gun (FEG) operating at 300 keV and equipped with a Gatan image filter QuantumER. CBED remains the most sensitive TEM technique to the strain because of the strong influence of the lattice parameters on the fine High Order Laue Zone (HOLZ) line positions. For a given zone axis [uvw], HOLZ lines appear as black deficiency lines in the transmitted diffraction disk and correspond to the various (hkl) planes being in exact Bragg conditions under the chosen orientation.[24] They can therefore be used to determine the crystal parameters.[25] In practice, the experimental HOLZ line positions are compared to dynamical diffraction simulations through the Hough transformation procedure,[26] so as to retrieve the lattice parameters in the selected region. For this experiment, N-beam dynamical simulations were performed using Java Electron Microscope Simulation (JEMS) software[27] while a homemade Hough transform code was implemented in Gatan Digital Micrograph. All the experimental CBED patterns were acquired in the [230] zone axis and were zero loss filtered with a 10 eV energy window. In addition to the lattice parameter, HOLZ line positions are also sensitive to the TEM accelerating voltage. Therefore, a CBED pattern obtained in the undoped (and undistorted) substrate at a depth of ~300 nm was initially simulated to determine the precise acceleration voltage of the e-beam (found equal to 299.1 kV, cf. Fig. SI-1 of the supplementary material)[28] and then used as a reference for the strain measurements. In CBED, the perpendicular strain in the doped region $\varepsilon_{\perp(CBED)}$ is measured with respect to the undoped Ge substrate lattice parameter a_{Ge} instead of the relaxed lattice parameter a_{rel} [cf. Eq. (1)]. In order to compare the CBED results with those obtained by HR-XRD, the following relation is therefore used:

$$\varepsilon_{\perp(\mathrm{CBED})} \cong \frac{a_\perp - a_{Ge}}{a_{Ge}} = \left(1 + \frac{C_{11}}{2C_{12}}\right)\varepsilon_\perp. \tag{3}$$

Figure 1 presents the cross section (CS-TEM) images from two samples annealed with an energy density of 0.80 [Fig. 1(a)] and 1.05 J/cm^2 [Fig. 1(b)]. The corresponding SIMS P depth concentration profiles are superimposed. After LTA at 0.80 J/cm^2, the implant damage was only partially recovered through the formation of a polycrystalline material in the surface region (down to a depth of about 25 nm). The formation of a polycrystalline structure is a clear hint of the incomplete melt of the initial amorphous layer, i.e., the liquid/solid interface never reaches the underlying crystal substrate during annealing. As a consequence, conventional end-of-range (EOR) defects [cf. white arrows in Fig. 1(a)] are formed in the region below the original amorphous layer, similarly to what occurs during anneals in the solid phase.[29]

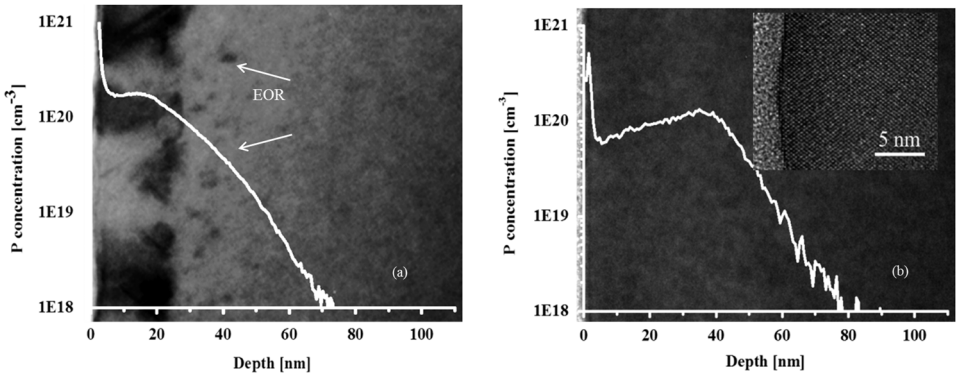


FIG. 1. SIMS profiles superposed to TEM images of samples after 0.80 (a) and 1.05 J/cm^2 (b) LTA. In the inset of (b), HRTEM indicates a perfectly recrystallized material.

In these conditions, negligible phosphorus diffusion is expected during LTA in the non-melted region, as indicated by the phosphorus SIMS profile, which is undistinguishable from the as-implanted one (not shown). On the other hand, a complete epitaxial recrystallization is reached after the 1.05 J/cm^2 process, as shown in Fig. 1(b), where the High Resolution TEM (HR-TEM) in the inset clearly proves an epitaxial growth without any trace of detectable defects. Indeed, in these conditions, the melted region extended below the original amorphous layer, allowing a liquid phase epitaxial regrowth from the underlying single-crystal substrate and a complete dissolution of the EOR. At such higher laser energy densities, SIMS analysis reveals a significant redistribution of P [cf. Fig. 1(b)] where the sharp decrease in the P concentration at about 40 nm provides an estimation of the maximum melt depth, with the diffusion coefficient in the solid phase being much lower than that in the liquid phase.[30,31] The complete set of P concentration profiles measured from all the annealed samples is reported in Fig. SI-2 of the supplementary material. The structural analyses discussed earlier give hints on the disorder induced by LTA at the nanoscale. Nonetheless, LTA treatment induces modifications on a scale that is several orders of magnitude larger compared to that explored by TEM. Complementary information on the damage recovery during LTA can therefore be obtained by Raman spectroscopy, as reported in the supplementary material. In particular, the effective doping inferred from the Raman spectra of the samples annealed at a high energy density (1.05 and 1.20 J/cm^2) was confirmed by Hall effect measurements.[18] In addition, the sheet carrier densities measured by the Hall effect were in good agreement with the integrated concentrations obtained by SIMS, indicating that the implanted dopants are fully electrically active in these samples, with concentrations as high as 1×10^{20} cm^{-3} (a summary of the electrical characterizations carried out on these samples and published in a previous study[18] is reported in Fig. SI-4 of the supplementary material). The two samples annealed at a high energy density are therefore perfectly suited for the investigation of the lattice deformation induced by the active phosphorus dopant atoms.

Strain measurements were therefore performed by HR-XRD and CBED. HR-XRD rocking curves were recorded from both samples (cf. Fig. SI-5 of the supplementary material). In both cases, the rocking curves exhibit a shoulder on negative angles, which, given the pseudomorphicity of the doped layers, indicates a positive perpendicular strain. The corresponding $\varepsilon_\perp$ strain depth profiles are reported in Fig. 2 (orange diamonds for the 1.05 J/cm^2 sample and red squares for the 1.20 J/cm^2 one). After a 1.05 J/cm^2 anneal, the estimated positive perpendicular strain is confined within a 48 ± 5 nm-thick surface layer with a maximum level of $\sim 8 \times 10^{-5}$ (91 ± 5 nm and $\sim 5 \times 10^{-5}$ for 1.20 J/cm^2). In both cases, the thickness of the strained layer corresponds to the maximum melt depth, while the strain levels are proportional to the corresponding atomic concentrations as measured by SIMS as shown by the fits reported in the figure.

Considering the extremely low strain levels investigated in this work (systematically below 10^{-4}), STEM-CBED measurements were also performed so that independent localized strain measurements could be achieved with nanometer depth resolution. CBED analyses were conducted on the 1.05 J/cm^2 sample to acquire ~20 experimental CBED patterns from different depths where varying levels of

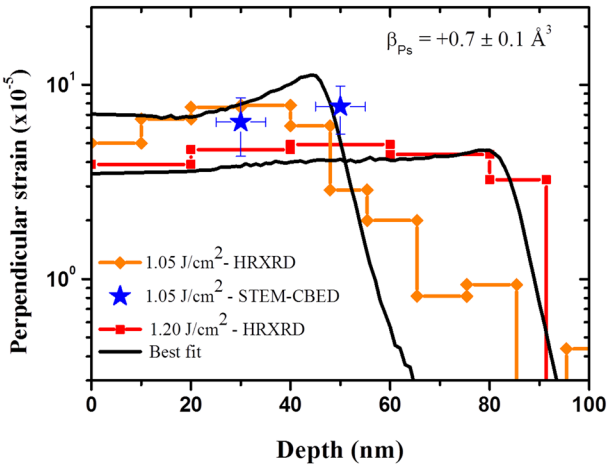


FIG. 2. Strain vs. depth profile as measured by means of HRXRD in P-doped Ge after LTA processes at 1.05 (orange diamonds), and 1.20 J/cm^2 (red squares). Data are compared with their fits (black lines) obtained as described in Fig. S1-7 of the supplementary material. Punctual strain measurements obtained by STEM-CBED after LTA at 1.05 J/cm^2 are also shown (blue stars).

doping concentration are attained.[32,33] Figure 3(a) presents the experimental CBED pattern at a depth of ~50 nm, close to the region with the highest P concentration. The corresponding N-beam dynamical simulated pattern, shown in Fig. 3(b), was calculated assuming a perpendicular positive strain $\varepsilon_{\perp(CBED)}$ of 0.018% [corresponding to the maximum perpendicular strain measured by HRXRD, cf. Eq. (1)] and provides a perfect fit to the experimental pattern. To highlight the small strain effect on the HOLZ line position, we superimpose in Fig. 3(c) the simulated CBED pattern of the strained area to the simulated CBED pattern of the strained area to HOLZ line positions extracted in the undistorted substrate [red lines in Fig. 3(c)], and the shift in the HOLZ line positions (indicated by the red arrows) clearly confirms an expansion of the lattice parameter.

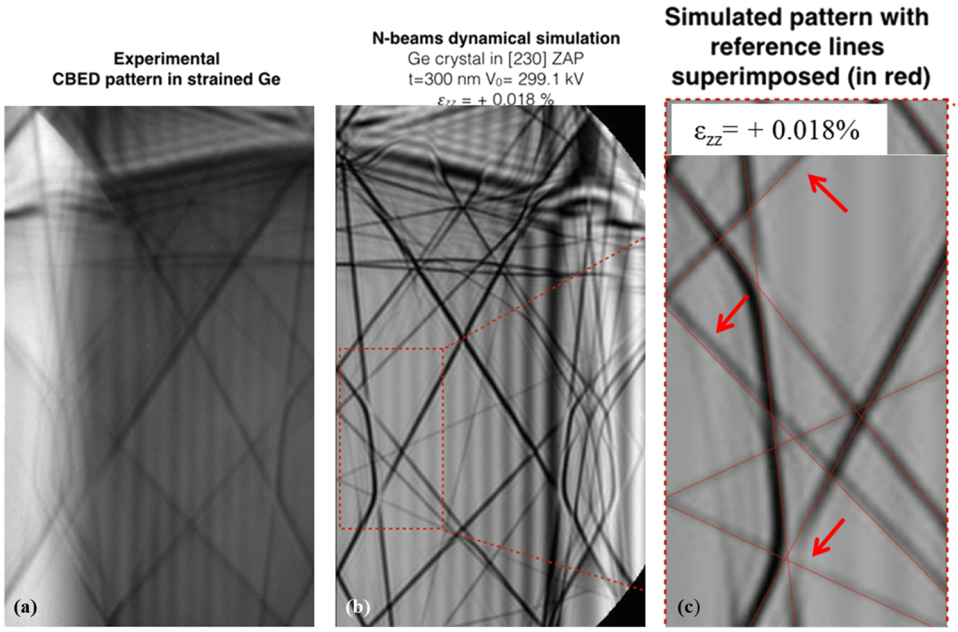


FIG. 3. Experimental (a) and simulated (b) CBED pattern taken at ~50 nm from the surface. The comparison between the N-beam dynamical simulated CBED patterns of the strained area (in gray) with the unstrained reference (in red) are reported in (c). The shift of HOLZ line positions, marked by arrows, is ascribed to a variation of lattice parameter.

The same analysis, repeated at a depth of ~30 nm (cf. Fig. SI-6 of the supplementary material), provided a slightly lower value for the perpendicular strain $\varepsilon_{\perp(CBED)}$ (0.015%), in agreement with the lower dopant concentration at this depth compared to ~50 nm. Given that in CBED the perpendicular strain in the doped region $\varepsilon_{\perp(CBED)}$ is measured with respect to the undoped Ge substrate lattice parameter a_{Ge}, the data have been converted to perpendicular strain with respect to the relaxed lattice parameter a_{rel} [cf. Eq. (3)]. Thus, the two perpendicular strain values determined by CBED were finally compared to those obtained by HRXRD (blue stars and orange diamonds in Fig. 2, respectively). It is striking to note the excellent agreement, within the error bars, between the values obtained by the two different, but complementary, techniques.

These results already provide a qualitative confirmation of the resulting lattice expansion of the Ge:P system. However, a more quantitative analysis can be performed considering that no contribution from other strain sources, such as inactive clusters or impurities, have been detected in these samples.[34] Indeed, since electrical characterizations have confirmed that the totality of the implanted dopants is electrically active, it is possible to reproduce the strain data starting from the corresponding SIMS profiles of P and using a unique scaling factor. (Attempts of resolving the effect from O impurities detected by SIMS measurements are reported in Fig. SI-7 of the supplementary material. The contribution is found negligible.) In this way, the strain per substitutional P atom, β_{Ps}, can be quantified by fitting the measured perpendicular strain depth profiles, $\varepsilon_{\perp}(z)$, by the following formula:

$$\varepsilon_{\perp}(z) = \beta_P C_P(z), \tag{4}$$

where $C_P(z)$ is the SIMS depth concentration profile of P. Indeed, a unique scaling factor of $\beta_{Ps} = +0.7 \pm 0.1$ Å^3 is able to reproduce the strain in the superficial recrystallized regions for both investigated samples, processed with different LTA conditions (cf. black lines in Fig. 3). Our results are in excellent agreement with *ab initio* calculations based on the Cargill-Keyes theory for the doping dependence of lattice parameters in semiconductors[15,16] that suggest $\beta_{Ps} \sim +0.5$ Å^3 [8,35] (cf. Fig. SI-8 of the supplementary material). Moreover, we are confident about the reliability of the β_{Ps} estimation, thanks to the very good crystal quality of the investigated samples (as evidenced by TEM and Raman analyses discussed earlier) and the very high incorporation of substitutional P (~1×10^{20} cm^{-3}).

In summary, in this work, we first presented a detailed structural investigation of P implanted and LTA annealed samples, showing how the damage recovery occurs as a function of the LTA conditions. In particular, after low energy density LTA, several residual defects and polycrystalline structure are left while the P dopant diffusion is negligible. On the other hand, high energy LTA results in full crystallization, with a maximum active dopant concentration up to ~1×10^{20} cm^{-3}. Strain investigations were performed on the fully activated samples and clearly indicate that, even in the Ge:P system, the electronic contribution to the lattice parameter modification is larger than the size mismatch contribution associated with the atomic radii. Such behavior, predicted by theory, is observed experimentally for the first time, thanks to the high sensitivity of the measurement techniques used in this work.

See supplementary material for the experimental CBED pattern and the corresponding simulation of the undistorted Ge substrate for the determination of the TEM accelerating voltage. Moreover, all the SIMS profiles of P-implanted samples subjected to LTA at energies ranging from 0.55 to 1.20 J/cm^2 are shown. A detailed Raman spectroscopy study elucidates the disorder recovery induced by LTA and is correlated with active carrier concentration measured by ECV. Supplementary HR-XRD rocking curves from samples annealed with 1.05 J/cm^2 and 1.20 J/cm^2 indicate positive perpendicular strain in agreement with the CBED pattern taken at ~30 nm from the surface. In addition, the contribution of other strain sources such as oxygen impurities is excluded by evaluating the dopant electrical activation and its strain contribution. Finally, our experimental strain values are compared with *Ab initio* theoretical ones shown in the literature.

The authors acknowledge G. Caruso, E. Bruno, and G. Faraci from the University of Catania, and V. Boureau, N. Cherkashin, and A. Claverie form CEMES-CNRS for helpful discussions.

R. Cours (CEMES) is acknowledged for FIB sample preparation. Finally, the authors wish to acknowledge the cooperation project between CNR and CNRS "Understanding and Modeling of Excimer Laser Annealing" (UMEX).

[1] C. Clays and E. Simoen, *Germanium-Based Technologies—From Materials to Devices* (Elsevier, Amsterdam, 2007).
[2] R. Pillarisetty, Nature **479**, 324–328 (2011).
[3] D. A. B. Miller, Proc. IEEE **97**, 1166–1185 (2009).
[4] J. Liu, Photonics **1**(3), 162–197 (2014).
[5] M. J. Adams and P. T. Landsberg, in *Proceedings of the 9th International Conference on the Physics of Semiconductors, Moscow* (Akademiya Nauk, 1968), p. 619.
[6] J. Liu, X. Sun, R. Camacho-Aguilera, L. C. Kimerling, and J. Michel, Opt. Lett. **35**, 679 (2010).
[7] R. Milazzo, E. Napolitani, G. Impellizzeri, G. Fisicaro, S. Boninelli, M. Cuscunà, D. De Salvador, M. Mastromatteo, M. Italia, A. La Magna, G. Fortunato, F. Priolo, V. Privitera, and A. Carnera, J. Appl. Phys. **115**, 053501 (2014).
[8] C. Xu, C. L. Seranatne, J. Kouvetakis, and J. Menéndez, Phys. Rev. B **93**, 041201(R) (2016).
[9] M. J. Suess, R. Geiger, R. A. Minamisawa, G. Schiefler, J. Frigerio, D. Chrastina, G. Isella, R. Spolenak, J. Faist, and H. Sigg, Nat. Photonics **7**, 466–472 (2013).
[10] R. Soref, Nat. Photonics **4**, 495–497 (2010).
[11] L. Baldassarre, E. Sakat, J. Frigerio, A. Samarelli, K. Gallacher, E. Calandrini, G. Isella, D. J. Paul, M. Ortolani, and P. Biagioni, Nano Lett. **15**, 7225–7231 (2015).
[12] R. G. Elliman and J. S. Williams, Curr. Opin. Solid State Mater. Sci. **19**, 49–67 (2015).
[13] A. R. Denton and N. W. Aschroft, Phys. Rev. A **43**, 3161–3164 (1991).
[14] J. Bardeen and W. Shockley, Phys. Rev. **80**(1), 72–80 (1950).
[15] G. S. Cargill, J. Angilello, and K. L. Kavanagh, Phys. Rev. Lett. **61**, 1748–1751 (1988).
[16] K. L. Kavanagh and G. S. Cargill, III, Phys. Rev. B **45**, 3323–3331 (1992).
[17] S. F. Lombardo, S. Boninelli, F. Cristiano, G. Fisicaro, G. Fortunato, M. G. Grimaldi, G. Impellizzeri, M. Italia, A. Marino, R. Milazzo, E. Napolitani, V. Privitera, and A. La Magna, Mater. Sci. Semicond. Process. **62**, 80–91 (2017).
[18] M. Shayesteh, D. O' Connell, F. Gity, P. Murphy-Armando, R. Yu, K. Huet, I. Toqué-Tresonne, F. Cristiano, S. Boninelli, H. H. Henrichsen, P. Folmer Nielsen, D. Hjorth Petersen, and R. Duffy, IEEE Trans. Electron Devices **61**(12), 4047–4055 (2014).
[19] E. Bruno, G. G. Scapellato, G. Bisognin, E. Carria, L. Romano, A. Carnera, and F. Priolo, J. Appl. Phys. **108**, 124902 (2010).
[20] J. C. H. Spence and J. M. Zuo, *Electron Microdiffraction* (Plenum Press, New York, 1992).
[21] V. Holý, U. Pietsch, and T. Baumbach, *High Resolution X-Ray Scattering from Thin Films and Multilayers* (Springer, Berlin, 1998).
[22] *Semiconductors-Basic Data*, edited by O. Madelung (Springer, Marburg, 1996), pp. 28–42.
[23] M. Wormington, C. Panaccione, K. M. Matney, and K. Bowen, Philos. Trans. R. Soc., A **357**, 2827 (1999).
[24] J. P. Morniroli, *Large-Angle Convergent-Beam Electron Diffraction (LACBED): Application to Crystal Defects* (French Society of Microscopies (S.F.μ), Paris, 2002).
[25] J. M. Zuo, Ultramicroscopy **41**, 211–223 (1992).
[26] S. Krämer and J. Mayer, J. Microsc. **194** (1), 2–11 (1999).
[27] P. A. Stadelmann, Ultramicroscopy **21**(2), 131–145 (1987).
[28] Y. P. Lin, D. M. Bird, and R. Vincent, Ultramicroscopy **27**(1), 233–240 (1989).
[29] S. Boninelli, G. Impellizzeri, A. Alberti, F. Priolo, F. Cristiano, and C. Spinella, Appl. Phys. Lett. **101**, 162103 (2012).
[30] M. Rousseau, P. B. Griffin, and J. D. Plummer, Appl. Phys. Lett. **65**, 578 (1994).
[31] G. Fortunato, L. Mariucci, M. Stanizzi, V. Privitera, C. Spinella, S. Coffa, and E. Napolitani, Mater. Sci. Semicond. Process. **4**, 417–423 (2001).
[32] L. Clément, R. Pantel, L. F. T. Kwakman, and J. L. Rouvière, Appl. Phys. Lett. **85**, 651–653 (2004).
[33] F. Houdellier, C. Roucau, L. Clément, J. L. Rouvière, and M. J. Casanove, Ultramicroscopy **106**, 951–959 (2006).
[34] R. Milazzo, G. Impellizzeri, D. Piccinotti, A. La Magna, G. Fortunato, D. De Salvador, A. Carnera, A. Portavoce, D. Mangelinck, V. Privitera, and E. Napolitani, J. Appl. Phys. **119**(4), 045702 (2016).
[35] A. V. G. Chizmeshya, C. Ritter, J. Tolle, C. Cook, J. Menendez, and J. Kouvetakis, Chem. Mater. **18**, 6266–6277 (2006).